Optotransduction Pathway, Exploring Connections with Inflammation

Alessandro Ravoni †, Veronica Paparozzi †, Tiziana Guarnieri †, Cecilia Sanzini, Luigi Manni, Christine Nardini *

Posted Date: 11 May 2026

doi: 10.20944/preprints202605.0627.v1

Keywords: optotransduction; photobiomodulation; inflammation; systems biology markup language; pathway; network biology

 doi:10.20944/preprints202605.0627.v1

Article

Optotransduction Pathway, Exploring Connections with Inflammation

Alessandro Ravoni [1,†], Veronica Paparozzi [1,†], Tiziana Guarnieri [1,2,3,†], Cecilia Sanzini [1,4], Luigi Manni [4] and Christine Nardini [1,*]

[1] Consiglio Nazionale delle Ricerche, Istituto per le Applicazioni del Calcolo "Mauro Picone", 00185 Roma, Italy

[2] Dipartimento di Scienze Biologiche, Geologiche e Ambientali (BIGEA), University of Bologna, 40100 Bologna, Italy

[3] Centro Interdipartimentale di Ricerca Industriale - CIRI Scienze della Vita e Tecnologie per la Salute, Università di Bologna, 40126 Bologna, Italy

[4] Consiglio Nazionale delle Ricerche, Istituto di Farmacologia Traslazionale, 00185 Roma, Italy

* Correspondence: christine.nardini@cnr.it

† These authors contributed equally to this work.

Abstract

The ability of cells to translate optical radiation into biochemical signals, i.e., optotransduction, plays an important role in emerging therapeutic strategies, with a relevant influence on inflammation. However, a systemic understanding of the molecular pathways underlying the transduction of these physical stimuli is still lacking. In this work, we present a molecular map of optotransduction reconstructed from the literature and provide its representation as pathway, using the standard Systems Biology Markup Language. This representation enables network-based analyses and allows us to investigate the differential effect of stimuli wavelengths and overlap with other forms of physical transduction, namely mechanotransduction.

Keywords: optotransduction; photobiomodulation; inflammation; systems biology markup language; pathway; network biology

1. Introduction

Signal transduction represents the fundamental process by which physical stimuli are converted into biochemical signals, enabling the transmission of information both within and between cells. In a cell, these stimuli interact with specific components, triggering responses or cascades of biochemical reactions essential for homeostasis and functional adaptation. In this work, we study the molecular mechanisms downstream the conversion of optical radiation beyond the specialized processes occurring in the eye. In the following, to emphasize the concept of transduction, while specifying it to optical radiation, we refer to the process as optotransduction (vs mechano and other types of physical transduction [1].

It was long believed that optical stimuli could exclusively influence specialized cells in the retina; more recent studies, however, have shown that skin cells such as fibroblasts, keratinocytes and melanocytes can detect sunlight through chromophores and a series of light-sensitive proteins called opsins [2–4]. Activation of these receptors can initiate a variety of intracellular signaling cascades that regulate multiple biological processes, including cell proliferation, pigmentation, stress responses and the modulation of inflammatory pathways [1,4,5]. Optotransduction therefore represents a key mechanism through which optical stimuli can be translated into functional changes in cellular behavior in a more systemic and impactful way, given the ubiquity of fibroblasts and the extension of skin.

 doi:10.20944/preprints202605.0627.v1

In the clinical landscape, the ability of tissues to respond to optical stimuli underlies several therapeutic approaches (in dermatology, neurology and regenerative medicine) based on controlled light exposure, including Photobiomodulation (PBM), Low-Level Laser Therapy (LLLT) [5–10] and more recently experimental greenlight exposure in (prodromal) Alzheimer patients [11], to name a few. These techniques involve the application of specific wavelengths, typically ranging from approximately 400 to 1200 nm, delivered at low power densities to induce photobiological effects without causing thermal damage or cytotoxicity. Among the most interesting outcomes reported in recent years is the potential anti-inflammatory effect associated with these therapies. Several studies have shown that tissues exposed to low-intensity light exhibit a local reduction in edema, oxidative stress markers, and pro-inflammatory cytokines [6]. Despite these clinical benefits, to our knowledge, the exact cellular signaling pathways responsible for these actions are not yet fully understood, in particular due to jeopardized information, lacking organization into a coherent systemic framework.

In this context, constructing a comprehensive representation of the molecular actors involved in optotransduction becomes particularly useful. In the present work, we integrated information scattered across the literature to build a systematic representation of the interactions between optical stimuli and inflammatory processes.

The identified molecular interactions have been organized within a network-based formalism, a mathematical approach at the basis of the well assessed Systems [12] and Network [13] Biology research areas that allows the complexity of biological systems to be captured by representing the multiple interactions occurring among the molecular entities involved. Networks or maps or graphs (G), can be formally represented by three sets namely nodes (N, representing the molecular entities) edges (E, representing the connections among molecular entities, like biochemical reactions) and attributes (A, that further qualify the nature of nodes and edges) G={N,E,A}. As such, graphs are well suited to represent biological pathways. To ensure uniformity, reliability, and reproducibility of the representation, here we adopt the Systems Biology Markup Language (SBML, [14]) to describe the graph, and the associated System Biology Graphical Notation (SBGN, [15]) for its graphical representation, as discussed in Methods.

This representation enables the so-called diffusion analysis [16] (see Section 2.3 for further details) to explore the differential biological processes elicited by distinct optical stimuli (mostly distinct wavelengths). Finally, the map allowed us to identify several points of overlap with the pathway of mechanotransduction recently updated by our group [17]. Given the very limited representation of the molecular aspects of physical transduction, this represents a unique opportunity to explore commonalities, potentially translating into alternatives for treatments (for a deeper discussion see [18]).

This work highlights the potential of standardized biological maps (a.k.a. in silico pathways) and supports the broader perspective of progressively integrating different representations of stimulus transduction mechanisms within a unified framework. The construction of the map is a result in itself, as it collects in one place the molecular actors involved in optotransduction. This represents the necessary condition to identify emergent properties, i.e., characteristics that become observable only when the system is studied in its complexity, in a variety of (future) applications. These include, for instance, integration with other relevant pathways (relevant drugs metabolism, diseases of interest etc.) for the personalized (patient-specific) identification of molecules of potential biomedical interest as markers or targets, that might remain hidden when analyzing isolated aspects of optotransduction [19].

2. Materials and Methods

2.1. Design of the Optotransduction Pathway

We collected the relevant literature [3,5–9,20–47] from PubMED (https://pubmed.ncbi.nlm.nih.gov/) and Google Scholar (https://scholar.google.com/) using the keywords “PBM”, “LLLT”, “Opsin”, “Phototransduction”, “Anti-inflammatory effects”,

 doi:10.20944/preprints202605.0627.v1

"Inflammation", and adding specific information on the Aryl Hydrocarbon Receptor, for its role as a mediator of environmental signals and inflammation [17].

All molecular entities and reactions mentioned in the literature were manually organized into the SBML Level 2 Version 4 format [14], a well-defined standard language used to represent in silico pathways in a human- and machine-readable format. This enables structured models' descriptions by organizing biochemical actors (species) and the processing governing their interactions (reactions) into eXtensible Markup Language (XML) data structures. The core components common to all SBML Levels and Versions consist of Compartment, Species and Reaction objects, hereafter referred to as entities in a broad sense. Each entity is defined by a set of mandatory and optional Attributes (e.g., "metaid", "id", "name") that among other functions ensure internal model referencing, as well as additional biological information incorporated through the Notes and Annotation tags. Detailed specifications are provided in the Supplementary Material. Notably, the Annotation element was employed to ensure standardized entities' identification in accordance with the MIRIAM [48] guidelines, by linking each entity to the appropriate external database resources. Reference databases for species were selected based on their biochemical nature: Universal Protein Knowledgebase (Uniprot, [49]) for proteins, National Center for Biotechnology Information Gene (NCBI, [50]) for genes, Chemical Entities of Biological Interest (ChEBI, [51]) for small molecules, Systems Biology Ontology (SBO, [52]) for stimuli, Gene Ontology (GO, [53]) Cellular Components sub ontology for cellular compartments.

To match these definitions to the general graph notation (G={N,E,A}) introduced in Section 1, an SBML model can be represented as a graph as follows: species correspond to the nodes N; reactions correspond to the edges E, where each edge may connect multiple nodes at either end (i.e., hyperedges) or link nodes (i.e., *modifier species* in SBML jargon) to an edge, as in the case of inhibition processes; while Notes and Annotation are encoded in the set A, and may be associated with both nodes and edges.

Model construction and graphical representation were performed using the CellDesigner [54] software (version 4.4.2), which exploits the SBML coupled with SBGN notations to enable a detailed illustration of a pathway components as well as a flexible representation of complex biochemical interactions. To guarantee maximum informativeness when representing molecular complexes, we distinguish between two classes of complexes: the first one corresponds to a biological complex (e.g., a protein complex), while the second one consists of a group of molecules which participate to a shared biological function (e.g., DNA damage, oxidative stress), herein referred to as a functional complex. To differentiate among distinct types of functional complexes, we adopted the notation defined by Reactome, employing the "Defined Set" and "Open Set" classifications respectively (see Supplementary Material for details). To avoid possible ambiguity in notation and to be compliant with the SBML jargon, hereafter we will refer to all interacting actors in the map (the nodes) as species, which include molecules, biological complexes, and functional complexes.

Overall, the constructed map consists of 7 compartments, 177 species, and 305 reactions.

2.2. Overlap in Cellular Signaling

As mentioned above, the availability of physical stimuli transduction pathways is very scarce. To the best of our knowledge, only mechanotransduction has been provided in SBML format, with a recent update by our group [17]. Since transduction of physical stimuli is known to share anti-inflammatory activity [18], we exploited the machine readable SBML representation to precisely search for such overlap, if any.

We used two different approaches to investigate these points of contact. The first, most intuitive approach, searches directly for overlapping nodes (i.e., species-level overlap) between the two pathways (Section 2.2.1). The second approach, more sophisticated, searches for shared connected nodes and edges (i.e., pathway-level overlap) between the two (Section 2.2.2).

In both approaches, the search relies on identical MIRIAM IDs, for complexes (recall that both biological and functional complexes are associated with more than one MIRIAM ID) this is

 doi:10.20944/preprints202605.0627.v1

generalized by considering two species from different maps to be *equivalent* if they share at least one MIRIAM ID That is:

$$n1 = n2 \Leftrightarrow M(n1) \cap M(n2) \neq \emptyset, \quad (1)$$

where we denote with M(n) the set of MIRIAM ID associated with species *n*.

2.2.1. Species-Level Overlap

The first approach identifies all the equivalent species in the two maps. To achieve this, we used the *tidysbml* R package [55], that extracts (among others) the list of all involved species and the related annotations from the SBML file. A simple overlap among the lists of species from the two maps identifies the shared molecules.

2.2.2. Pathway-Level Overlap

The second approach uses the dedicated MIMO software [56] to identify more subtle overlaps, by collecting the set of pathways (sets of nodes and connected edges) that involve equivalent species in both maps. MIMO allows users to define a list of constraints for the computation of the overlap. In particular, the equivalence between species can be limited *a priori*, with exclusion criteria, which in our case are defined as follows:

In our map, optical stimuli are all identified by the same MIRIAM ID (SBO:0000405, perturbing agent), regardless of the specific characteristics (wavelength, energy etc.),as the most appropriate term, with no other specifiers. Therefore, equivalence between such species is systematically excluded *a priori* in all analyses;

Small molecules, with ChEBI ID, may or may not be explicitly represented in a map, depending on the level of resolution adopted in the literature to describe a given process. This may thus affect the overlap analysis in an uncontrolled manner. For this reason, we perform two separate analyses: one labeled *small molecules included* (SMI), in which small molecules are matched, and one labeled *small molecules excluded* (SME), in which the equivalence between small molecules is explicitly excluded *a priori*.

Additional criteria include:

Information about the compartments to which each species belongs, that is, by allowing a match between equivalent species only if there is also a match between their associated compartments (case labeled as YC), or by ignoring compartment information altogether (case labeled as NC);

Finally, the pathways from different maps are not required to be identical up to a user-defined length L. L indicates the pathway length, i.e., the number of edges that separate the nodes (molecules) of interest. That is, two pathways are considered similar and included in the overlap if they connect equivalent species, regardless of the similarity between the intermediate species involved in up to L reactions (edges) along the path (i.e., the set of edges connecting one node/specie to another). The latter is particularly relevant in the case of the intersection between the optotransduction and mechanotransduction maps, as it allows the overlap to be estimated regardless of possible differences in the granularity of the pathway representations introduced during the reconstruction of the maps from the literature.

Overall, two species from different maps are considered equivalent for the purpose of the overlap analysis performed with MIMO if Equation 1 is satisfied and if their equivalence has not been explicitly excluded *a priori* by the above 4 criteria. In summary, by taking into account all possibilities relevant to us, we performed 4 comparisons for each length L, shown in the results section and in Supplementary Materials, including further details on the use of MIMO.

2.3. Diffusion Analysis

Diffusion analysis is a widely used network-based method to identify subsets of nodes that are close to each other within a network [16]. In a nutshell, the method propagates a signal starting from a (set of) input node(s) through the connections (edges) of the network, producing a proximity

 doi:10.20944/preprints202605.0627.v1

ranking that is specific to the wiring that represent the system modeled by the network, and that can be used to assess which nodes participate in the same transmission of information. In our case, we are interested in analyzing how optical stimuli propagate within the network, and which nodes are ultimately perturbed, since this translates into a proxy of the molecules affected by a given stimulus.

We perform diffusion analysis using both individual input nodes as directly extracted from the literature (identified by ID = SBO:0000405 and shown in Table S1 of the Supplementary Material) as well as sets of these nodes grouped according to the electromagnetic spectrum standard division, namely Green light (input nodes: Green, 532 nm), Red light (input nodes: 628 nm, 633 nm, 632.8 nm, 635 nm, 650 nm, 660 nm, 670 nm), and Near-IR (input nodes: NIR, 780 nm, 800 nm, 805 nm, 810 nm, 830 nm, 1068 nm, 1072 nm). We excluded from the analysis stimuli expressed in terms of energy (J) and absorbed dose (mGy). The analysis is performed using the built-in diffusion function of Cytoscape [57] using standard settings. For each input, we collect the species along with a ranking quantifying how strongly the signal propagates and use this preranked list to perform GSEA [58] GO enrichment analysis. The enrichment analysis is carried out using the GSEApy library [59], which returns a set of cellular processes associated with the provided species. From these, we retain only the statistically significant terms (q-value < 0.05).

3. Results and Discussion

3.1. Optotransduction Map

The map is available in two SBML files (optotransduction-core_celldesigner.xml and optotransduction-core_sbml.xml) generated using CellDesigner included in the Supplementary Material and publicly available in the BioModels repository under the identifier MODEL2604100001, where future extensions and updates will also be made available. Additional details, including the description of the differences between the two files, is provided in the Supplementary Material.

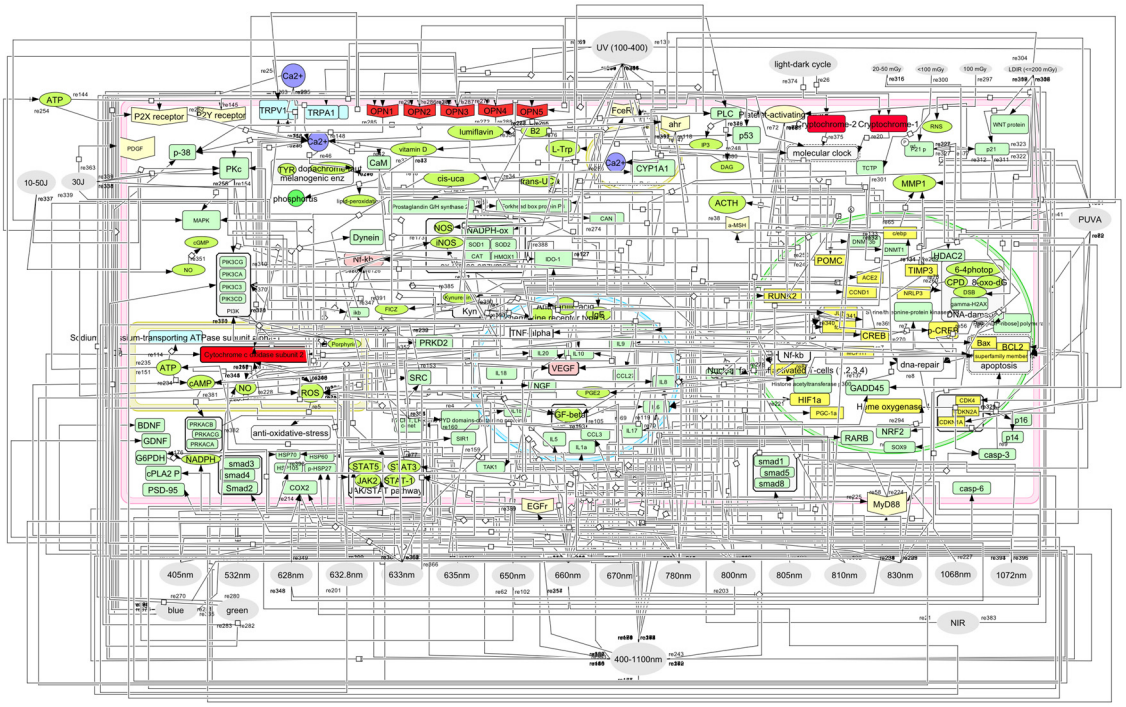

Figure 1. Representation of the optotransduction pathway as visualized in CellDesigner. Boxes represent compartments, arrows indicate reactions, and nodes represent species, using different shapes to distinguish different classes (green ovals for simple molecules, purple circles for ions, rounded rectangles for proteins, six-sided polygons for receptors, etc.; the full legend can be found in the CellDesigner manual). The grey nodes outside of the pink-outlined box (cell membrane) represent stimuli: inner nodes correspond to specific

 doi:10.20944/preprints202605.0627.v1

wavelengths, outer nodes correspond to ranges. High-resolution and searchable versions are provided in Figure S1 and the optotransduction-core_celldesigner.xml file, respectively. Both are available in the Supplementary Material and at biomodels.org (MODEL2604100001).

3.2. Mechano & Opto – Transduction Shared Pathways

3.2.1. Species-Level Overlap

Table 1 lists the species in the optotransduction and mechanotransduction maps for which there is a match between the associated (sets of) MIRIAM IDs, in accordance with Equation 1. Matches involving small molecules (i.e., species whose MIRIAM ID is a ChEBI identifier) are excluded from Table 1, for the sake of readability. A comprehensive list of all matches is provided in Table S2 of the Supplementary Material.

Table 1. Species match between the optotransduction and mechanotransduction maps based on MIRIAM IDs. *Indicates both the protein and its phosphorylated form, respectively.

Optotransduction map		**Mechanotransduction map**	
Name (map id)	**MIRIAM ID**	**Name (map id)**	**MIRIAM ID**
Nuclear factor NF-kappa-B (s22)	P19838_Q00653	S18 (s18)	P25963_P19838
		NFKB1 (s15; s16)	P19838
		p65/p50 dimer(s852)	Q04206_P19838
Dna-repair (s38)	O00206_Q99836	TLR 4 (s623)	O00206
Ox-stress enzymes (s63)	P00441_P04179_P04040_P09601_P35228_Q9Y5S8	SODM (s849)	P04179
AHR (s83)	P35869	AHR (s911)	P35869
		S917 (s917)	P27540_P35869
TNFA (s117)	P01375	TNFA (s937)	P01375
MAPK (s143)	P27361_P28482_Q16539_Q15759_P53778_O15264_P45983_P45984_P53779	MK08 (s570)	P45983
		*ERK1/2 (s957; s961)	P27361_P28482
		P38 (s956)	Q16539_O15264_Q15759_P5377
Nuclear factor NF-kappa-B (s170)	Q00653_P19838	S18 (s18)	P25963_P19838
		NFKB1 (s15; s16)	P19838
		p65/p50 dimer(s852)	Q04206_P19838
P2Y purinoceptor (s179)	Q9H244_Q9BPV8_Q15077_P47900_P51582_P41231_Q96G91_Q86VZ1	P2RY2 (s58)	P41231
		Complex1 (s65)	CHEBI%3A15422_P41231
JAK/STAT pathway (s253)	O60674_P42224_P40763_P42229	JAK2 (s872)	O60674
		STAT1 (s873)	P42224
		STAT3 (s874)	P40763
CYP1A1 (s272)	P04798	CYP1A1 (s920)	P04798
SRC (s273)	P12931	Complex3 (s842)	P12931_Q05397
		SRC (s912)	P12931
*CREB (s282; s284)	P16220_O43889_Q02930	CREB1 (s831)	P16220
HIF1a (s287)	Q16665	HIF1a (s561; s945)	Q16665
smad1-5-8 (s292)	Q15797_Q99717	*SM1/5 (s803; s804)	Q15797_Q99717_Q13485
p-38 (s297)	Q16539_O15264_Q15759_P53778	p38 (s956)	Q16539_O15264_Q15759_P5377
CCND1 (s310)	595	CCND1 (s193)	595
Smad (s345)	Q15796_P84022_Q13485	*SM2/3 (s733; s844)	Q15796_P84022_Q13485

 doi:10.20944/preprints202605.0627.v1

		*SM1/5 (s803; s804)	Q15797_Q99717_Q13485
PI3K (s360)	P42336_O00329_P48736_Q8NEB9	PK3CG (s836)	P48736
SIR1 (s366)	Q96EB6	SIR1 (s826)	Q96EB6
CAMP-dependent protein kinase catalytic (s367)	P17612_P22694_P22612	KAPCB (s830)	P22694
SOX9 (s372)	P48436	SOX9 (s832) s924 (s924)	P48436 P48436_Q13950
IL1B (s380)	P01584	IL1B (s939)	P01584
IL8 (s384)	P10145	IL8 (s940)	P10145
IL6 (s385)	P05231	IL6 (s946)	P05231
TGF-beta (s390)	P01137_P61812_P10600	TGFB (s525)	P01137

3.2.2. Pathway-Level Overlap

The overlap analysis performed with MIMO provides different results depending on the constraints and the input length L. From a preliminary analysis, we observed that the maximum pathway length in both the optotransduction and mechanotransduction maps is L=15. For this reason, in both SMI and SME, we performed the overlap analysis with MIMO using pathway lengths L ranging from 1 to 15 as shown in Table 2.

Overall, we found that the configuration providing the richest information, i.e., the most biologically interpretable results in terms of associated biological functions, is the one defined by the SMI and YC constraints with input length L = 3 as shown in Figure 2. Increasing L does not lead to a larger overlap (Figure S2 in the Supplementary Material).

Table 2. Summary of pathway-level overlap analysis. For each configuration of imposed constraints, the minimum input length that maximizes the number of species in the overlap is reported, along with the corresponding number of species. This number does not increase as L increases.

Configuration	Small molecules	Compartments	Minimum L	Overlap size
SMI - YC	Included	Included	3	6
SMI - NC	Included	Excluded	7	10
SME - YC	Excluded	Included	1	2
SME - NC	Excluded	Excluded	7	4

The overlap illustrated in Figure 2 shows that there is a common intracellular signaling machinery converging on calcium- and redox-dependent inflammatory mechanisms. Both types of stimuli converge towards cytosolic Ca^{2+} as a common second messenger, regulated by its extracellular influx and by inositol 1,4,5-trisphosphate (IP3)-mediated release from endoplasmic reticulum stores. This signaling pathway is closely related to the production of mitochondrial reactive oxygen species (ROS), thereby forming a bidirectional amplification loop for signal transduction. Downstream of these events, activation of stress kinases like p38 MAPK and transcription factors like NF-κB and HIF1α is observed, leading to the generation of inflammatory mechanisms. This shows that, in an inflammatory milieu, different types of physical stimuli - mechanical and optic - are integrated through a common signaling architecture involving Ca^{2+}-ROS-MAPK- NF-κB- HIF1α, with the mitochondrion acting as an integrator. In particular: ROS and Ca^{2+} act as second messenger that can be stimulated by both mechanical and optic stimuli; mitochondria are the core, as they produce ROS and NO, sense light through cytochrome oxidase and are sensitive to shear-stress; p38MAPK and NF-κB are common pro-inflammatory actors, linking optic and mechanical stimuli to inflammation; HIF1α is stabilized by ROS and mechanical stress.

 doi:10.20944/preprints202605.0627.v1

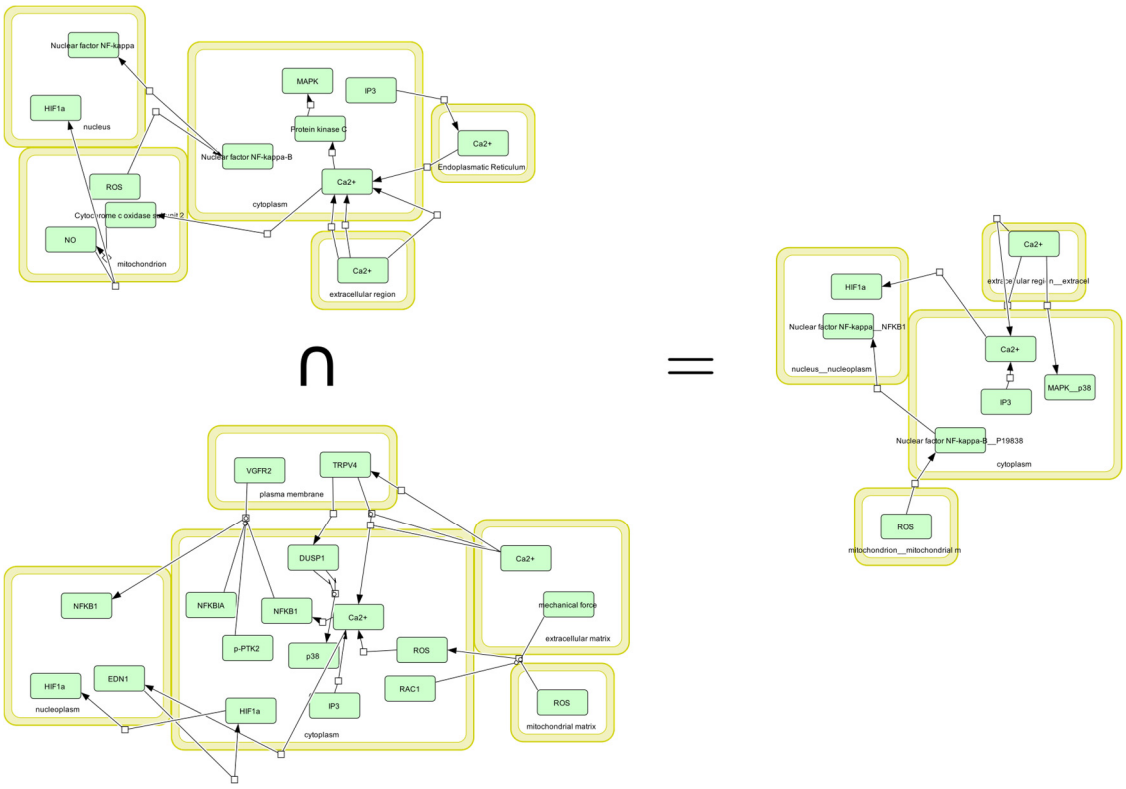

Figure 2. Overlap between the optotransduction and mechanotransduction maps obtained with MIMO**.** The figure reports the species from the optotransduction map involved in the overlap (upper left), the species from the mechanotransduction map involved in the overlap (bottom left), and the overlap between the two maps (right).

In addition to these predominantly pro-inflammatory aspects, specific components can mediate anti-inflammatory effects. In particular: in mechanotransduction, a low intensity stimulus (i.e., gentle mechanical strain) induces high expression of DUSP1 [60], which dephosphorylates p38 and JNK, limiting their inflammatory signalling with negative feedback that can be anti-inflammatory. The portion of the mechanotransduction map that incorporates this specific pathway, is shown in the Supplementary Materials, driven by stretch inputs. This signal follows the sequence stretch -> TRPV4 -> DUSP1. Consequently, DUSP1 acts as a direct regulator of p38 and JNK (MK08) signaling.

In optotransduction, a low intensity optical stimulus (i.e.,: low-level light therapy, photobiomodulation) induce a low expression of NO and activates cytocrome c oxydase. Low/moderate NO can be anti-inflammatory, as it inhibits NF-κB and reduces adhesion molecules, while high NO is pro-inflammatory; mitochondrial cytochrome c oxidase, when activated by certain light wavelengths (i.e.,: photobiomodulation), increases ATP, reduces ROS, and can lower inflammation via mitochondrial retrograde signalling. In the optotransduction map, this connection is evident and similarly reported in the Supplementary Materials. Specifically, red light and NIR stimuli, associated with low-level light therapy and photobiomodulation, are directly linked to cytochrome c oxidase subunit 2, which in turn is directly coupled to ROS and ATP production. These stimuli are also linked to NO through a signaling network involving Vascular Endothelial Growth Factor, oxidative stress enzymes, and cytochrome c oxidase subunit 2, and NO is eventually connected to NF-κB via IKB and AP-1 signaling.

Thus, mechanotransduction has a possible anti-inflammatory effect, mainly linked to high DUSP1 expression, while optotransduction has two putative anti-inflammatory mechanisms, such as NO-dependent inhibition of NF-κB and light-induced mitochondrial modulation that may counterbalance the pro-inflammatory signals. These mechano- and opto- triggered paths converging to a similar anti-inflammatory activity could help framing therapeutic alternatives, tailored to patients' needs or preferences or clinical and cultural environments

 doi:10.20944/preprints202605.0627.v1

3.3. (Diffusion Analysis) Exploring Differential Biological Effects of Wavelegths

The diffusion analysis of the optotransduction network reveals both shared and distinct patterns (enriched GO biological processes) for a subset of input nodes, namely 405 nm (UVA), 532 nm (green light), 650 nm (red light), and 400–1100 nm (visible + near-IR). Table 3 shows the obtained results; full details can be found in Tables S3 of SupplementaryTables.xlsx).

Table 3. Results of the enrichment analysis sorted by statistical significance, performed from the diffusion analysis output. Term and ID columns: GO cellular process. Lead Genes: genes contributing most to the enrichment score. Stimulus: name of the stimulus used in the diffusion. FDR q-val: q-value (adjusted False Discovery Rate) for each stimulus enrichment. In bold the GO term in common to all stimuli.

GO Term	GOID	Lead genes	Stimulus	FDR q-val
Negative Regulation of Macromolecule Biosynthetic Process	GO:0010558	SIRT1, CXCL8, TNF	400-1100 nm	0.023
Cellular Response to Tumor Necrosis Factor	GO:0071356	SIRT1, CXCL8, TNF, TP53	400-1100 nm 650 nm UVA	0.027 0.012 0.014
Regulation of Cell Adhesion	GO:0030155	SRC, CXCL8, TNF	400-1100 nm	0.031
Response to Peptide Hormone	**GO:0043434**	**CRY1, SRC, SIRT1**	**400-1100 nm** **532 nm** **650 nm** **UVA**	**0.039** **0.048** **0.029** **0.001**
Negative Regulation of Signal Transduction	GO:0009968	CRY1, CXCL8, TNF	400-1100 nm	0.047
Negative Regulation of Gene Expression	GO:0010629	HSPA1B, SIRT1, TNF, CXCL8	532 nm 650 nm UVA	0.044 0.005 0.026
Negative Regulation of Cellular Component Organization	GO:0051129	SRC, HSPA1B, TNF	532 nm UVA	0.049 0.032

Other inputs, as well as aggregated stimuli (Green Light, Red Light, and Near-IR, introduced in Section 2.3) do not yield significant results. It may surprise that specific wavelengths within a small range do not share the same type of enrichment. This is most likely due to how studies vary, for example, in their objectives, experimental technology and research question, often involving measurement limited to known/associated key molecules, while others may be neglected or overlooked. The way in which processes are explored across studies impact on the resulting network topology and in turn to different levels of heterogeneity in the connections between input nodes and other species in the map, resulting in a broader or more restricted propagation of the diffusion signal, and ultimately in the results of the enrichment analysis.

With respect to the enrichment results, we observe that *Response to Peptide Hormone (GO:0043434)*, is enriched for all four stimuli. The lead genes, CRY1, SRC and SIRT1 are involved in circadian regulation and signaling pathways connected to light response. They could be considered

 doi:10.20944/preprints202605.0627.v1

as an integrative hub where CRY1, a core component of the circadian clock, links the external stimuli (400-1100nm, 650nm, and 405 nm) to the internal circadian clock, thus allowing its setting (entrainment). SRC is a non-receptor influencing several core processes through kinase-mediated signals. In the context of *Response to Peptide Hormone*, it could be a signal integrator/amplifier that, following the exposition to different wavelengths radiation, translates the light input from CRY1 and the metabolic input from SIRT1 into kinase-mediated signaling. In particular, SRC could potentiate the cellular response to a concurrent peptide hormone signal, thereby influencing its metabolic action in a light-entrained way.

In the following, enrichment results are discussed in a stimulus-centric perspective, to better highlight their similarities and differences. The analysis of these profiles will assume that negative regulation processes suggest suppressive or protective roles; cellular responses to TNF indicate inflammatory modulation; peptide hormone response suggests metabolic/endocrine effects; cell adhesion regulation impacts tissue organization.

400–1100 nm (visible + near-IR). The dominant effect of this broadband stimulus is negative regulation (biosynthesis and signaling) coupled with stress responses (TNF, hormone) and adhesion control. This suggests a protective, anti-inflammatory, and metabolically integrative role.

650 nm (red light). Red light predominantly negatively regulates gene expression and modulates TNF/hormone responses. Compared to 400-1100 nm, red light stimulus appears more focused on transcriptional control in a context of stress response.

532 nm (green light). Green light has the weakest overall enrichment (FDR values near 0.05). Its effect is a possible negative regulation of transcription (negative regulation of gene expression) and cellular component organization, suggesting a role in stabilizing cell architecture under stress (response to peptide hormone).

UVA. UVA most strongly activates peptide hormone response (FDR = 0.001) and also robustly regulates TNF signaling, gene expression, and cell organization. Its effects are broader and more potent than green light, though narrower than 400-1100 nm (which uniquely affects macromolecule biosynthesis and signal transduction regulation). The overall effect of UVA is a negative control of transcription (negative regulation of gene expression) and cellular architecture (negative regulation of cellular component organization) under conditions of cell stress (cellular response to TNF/response to peptide hormone).

Additional information on this analysis is provided in Supplementary Materials.

4. Conclusion

Our work offers several novelties of interest for the biomdeical community concerned with the usage/effects of optical stimuli. First of all we offer a carefully curated pathway of optotransduction, to the best of our knowledge this is the first attempt to integrate in the standard SBML format relevant and scattered information on this biological function. Second, we explore the overlap of optotransduction with mechanotransduction, and identify a relevant mechanism associated to inflammation, whose activation can potentially be reconciled to optical or mechanical stimuli. The convergence of mechano- and opto- triggered paths to a similar anti-inflammatory activity offer a very interesting applicative perspective: this could help framing therapeutic alternatives, personalized not only to patients' needs but also to clinical and cultural contexts. Finally, we explore the differential biological effects of different wavelengths, offering a first characterization with potential biomedical interest. Although this work clearly requires experimental and clinical validations, it represents an mean to produce relevant hypotheses to be tested in an informed (and hence more cost-effective) manner.

Supplementary Materials: The following supporting information can be downloaded at the website of this paper posted on Preprints.org.

Institutional Review Board Statement: Not applicable.

 doi:10.20944/preprints202605.0627.v1

Informed Consent Statement: Not applicable.

Data Availability Statement: The data presented in this study are openly available in [Biomodels.org] [https://www.biomodels.org/search?query=MODEL2604100001] [MODEL2604100001].

Conflicts of Interest: The authors declare no conflict of interest.

References

1. Paparozzi, V.; Hooshmandabbasi, R.; Ravoni, A.; Ma, Y.; Manni, L.; Koh, T.J.; Maake, C.; Guarnieri, T.; Lai, D.; Zablotskii, V.; et al. Anti-Inflammatory Effects of Physical Stimuli: The Central Role of Networks in Shaping the Future of Pharmacological Research. *British Journal of Pharmacology* **2026**, *183*, 2177–2196, doi:10.1111/bph.70129.
2. Young, A.R. Chromophores in Human Skin. *Phys Med Biol* **1997**, *42*, 789–802, doi:10.1088/0031-9155/42/5/004.
3. Suh, S.; Choi, E.H.; Atanaskova Mesinkovska, N. The Expression of Opsins in the Human Skin and Its Implications for Photobiomodulation: A Systematic Review. *Photodermatol Photoimmunol Photomed* **2020**, *36*, 329–338, doi:10.1111/phpp.12578.
4. de Assis, L.V.M.; Tonolli, P.N.; Moraes, M.N.; Baptista, M.S.; de Lauro Castrucci, A.M. How Does the Skin Sense Sun Light? An Integrative View of Light Sensing Molecules. *Journal of Photochemistry and Photobiology C: Photochemistry Reviews* **2021**, *47*, 100403, doi:10.1016/j.jphotochemrev.2021.100403.
5. Tam, S.Y.; Tam, V.C.W.; Ramkumar, S.; Khaw, M.L.; Law, H.K.W.; Lee, S.W.Y. Review on the Cellular Mechanisms of Low-Level Laser Therapy Use in Oncology. *Front Oncol* **2020**, *10*, 1255, doi:10.3389/fonc.2020.01255.
6. Hamblin, M.R. Mechanisms and Applications of the Anti-Inflammatory Effects of Photobiomodulation. *AIMS Biophys* **2017**, *4*, 337–361, doi:10.3934/biophy.2017.3.337.
7. de Freitas, L.F.; Hamblin, M.R. Proposed Mechanisms of Photobiomodulation or Low-Level Light Therapy. *IEEE Journal of Selected Topics in Quantum Electronics* **2016**, *22*, 348–364, doi:10.1109/JSTQE.2016.2561201.
8. Serrage, H.; Heiskanen, V.; Palin, W.M.; Cooper, P.R.; Milward, M.R.; Hadis, M.; Hamblin, M.R. Under the Spotlight: Mechanisms of Photobiomodulation Concentrating on Blue and Green Light. *Photochem Photobiol Sci* **2019**, *18*, 1877–1909, doi:10.1039/c9pp00089e.
9. Leyane, T.S.; Jere, S.W.; Houreld, N.N. Cellular Signalling and Photobiomodulation in Chronic Wound Repair. *Int J Mol Sci* **2021**, *22*, 11223, doi:10.3390/ijms222011223.
10. Fernandes, F.; Oliveira, S.; Monteiro, F.; Gasik, M.; Silva, F.S.; Sousa, N.; Carvalho, Ó.; Catarino, S.O. Devices Used for Photobiomodulation of the Brain—a Comprehensive and Systematic Review. *Journal of NeuroEngineering and Rehabilitation* **2024**, *21*, 53, doi:10.1186/s12984-024-01351-8.
11. Feng, Q.; Chen, L.; Li, L.; Yang, J.; Wu, J.; Yue, Y.; Wang, Z. A Study of the Efficacy of 500nm Blue-green Light Therapy on Cognition, Mood, and Sleep in Prodromal Alzheimer's Disease. *Alzheimers Dement* **2025**, *20*, e088968, doi:10.1002/alz.088968.
12. Kitano, H. Systems Biology: A Brief Overview. *Science* **2002**, *295*, 1662–1664, doi:10.1126/science.1069492.
13. Barabási, A.-L.; Oltvai, Z.N. Network Biology: Understanding the Cell's Functional Organization. *Nat Rev Genet* **2004**, *5*, 101–113, doi:10.1038/nrg1272.
14. Hucka, M.; Bergmann, F.T.; Dräger, A.; Hoops, S.; Keating, S.M.; Novère, N.L.; Myers, C.J.; Olivier, B.G.; Sahle, S.; Schaff, J.C.; et al. Systems Biology Markup Language (SBML) Level 2 Version 5: Structures and Facilities for Model Definitions. *Journal of Integrative Bioinformatics* **2015**, *12*, 731–901, doi:10.1515/jib-2015-271.
15. Novère, N.L.; Hucka, M.; Mi, H.; Moodie, S.; Schreiber, F.; Sorokin, A.; Demir, E.; Wegner, K.; Aladjem, M.I.; Wimalaratne, S.M.; et al. The Systems Biology Graphical Notation. *Nat Biotechnol* **2009**, *27*, 735–741, doi:10.1038/nbt.1558.
16. Carlin, D.E.; Demchak, B.; Pratt, D.; Sage, E.; Ideker, T. Network Propagation in the Cytoscape Cyberinfrastructure. *PLoS Comput Biol* **2017**, *13*, e1005598, doi:10.1371/journal.pcbi.1005598.

 doi:10.20944/preprints202605.0627.v1

17. Suriyagandhi, V.; Ma, Y.; Paparozzi, V.; Guarnieri, T.; Di Pietro, B.; Dimitri, G.M.; Tieri, P.; Sala, C.; Lai, D.; Nardini, C. Mechanotransduction and Inflammation: An Updated Comprehensive Representation. *Mechanobiology in Medicine* **2025**, *3*, 100112, doi:10.1016/j.mbm.2024.100112.
18. Paparozzi, V.; Hooshmandabbasi, R.; Ravoni, A.; Ma, Y.; Manni, L.; Koh, T.J.; Maake, C.; Guarnieri, T.; Lai, D.; Zablotskii, V.; et al. Anti-Inflammatory Effects of Physical Stimuli: The Central Role of Networks in Shaping the Future of Pharmacological Research. *Br J Pharmacol* **2025**, doi:10.1111/bph.70129.
19. Maturo, M.G.; Soligo, M.; Gibson, G.; Manni, L.; Nardini, C. The Greater Inflammatory Pathway-High Clinical Potential by Innovative Predictive, Preventive, and Personalized Medical Approach. *EPMA J* **2020**, *11*, 1–16, doi:10.1007/s13167-019-00195-w.
20. Salehpour, F.; Mahmoudi, J.; Kamari, F.; Sadigh-Eteghad, S.; Rasta, S.H.; Hamblin, M.R. Brain Photobiomodulation Therapy: A Narrative Review. *Mol Neurobiol* **2018**, *55*, 6601–6636, doi:10.1007/s12035-017-0852-4.
21. de Assis, L.V.M.; Tonolli, P.N.; Moraes, M.N.; Baptista, M.S.; de Lauro Castrucci, A.M. How Does the Skin Sense Sun Light? An Integrative View of Light Sensing Molecules. *Journal of Photochemistry and Photobiology C: Photochemistry Reviews* **2021**, *47*, 100403, doi:10.1016/j.jphotochemrev.2021.100403.
22. Barolet, D.; Christiaens, F.; Hamblin, M.R. Infrared and Skin: Friend or Foe. *J Photochem Photobiol B* **2016**, *155*, 78–85, doi:10.1016/j.jphotobiol.2015.12.014.
23. Bathini, M.; Raghushaker, C.R.; Mahato, K.K. The Molecular Mechanisms of Action of Photobiomodulation Against Neurodegenerative Diseases: A Systematic Review. *Cell Mol Neurobiol* **2022**, *42*, 955–971, doi:10.1007/s10571-020-01016-9.
24. Becker, A.; Klapczynski, A.; Kuch, N.; Arpino, F.; Simon-Keller, K.; De La Torre, C.; Sticht, C.; van Abeelen, F.A.; Oversluizen, G.; Gretz, N. Gene Expression Profiling Reveals Aryl Hydrocarbon Receptor as a Possible Target for Photobiomodulation When Using Blue Light. *Sci Rep* **2016**, *6*, 33847, doi:10.1038/srep33847.
25. Buscone, S.; Mardaryev, A.N.; Raafs, B.; Bikker, J.W.; Sticht, C.; Gretz, N.; Farjo, N.; Uzunbajakava, N.E.; Botchkareva, N.V. A New Path in Defining Light Parameters for Hair Growth: Discovery and Modulation of Photoreceptors in Human Hair Follicle. *Lasers Surg Med* **2017**, *49*, 705–718, doi:10.1002/lsm.22673.
26. Caterina, M.J.; Pang, Z. TRP Channels in Skin Biology and Pathophysiology. *Pharmaceuticals (Basel)* **2016**, *9*, 77, doi:10.3390/ph9040077.
27. Chen, A.C.-H.; Arany, P.R.; Huang, Y.-Y.; Tomkinson, E.M.; Sharma, S.K.; Kharkwal, G.B.; Saleem, T.; Mooney, D.; Yull, F.E.; Blackwell, T.S.; et al. Low-Level Laser Therapy Activates NF-kB via Generation of Reactive Oxygen Species in Mouse Embryonic Fibroblasts. *PLOS ONE* **2011**, *6*, e22453, doi:10.1371/journal.pone.0022453.
28. Dompe, C.; Moncrieff, L.; Matys, J.; Grzech-Leśniak, K.; Kocherova, I.; Bryja, A.; Bruska, M.; Dominiak, M.; Mozdziak, P.; Skiba, T.H.I.; et al. Photobiomodulation-Underlying Mechanism and Clinical Applications. *J Clin Med* **2020**, *9*, 1724, doi:10.3390/jcm9061724.
29. Ferraresi, C.; Huang, Y.-Y.; Hamblin, M.R. Photobiomodulation in Human Muscle Tissue: An Advantage in Sports Performance? *Journal of Biophotonics* **2016**, *9*, 1273–1299, doi:10.1002/jbio.201600176.
30. Guarnieri, T. Hypothesis: Emerging Roles for Aryl Hydrocarbon Receptor in Orchestrating CoV-2-Related Inflammation. *Cells* **2022**, *11*, 648, doi:10.3390/cells11040648.
31. Guo, B.; Zhang, M.; Hao, W.; Wang, Y.; Zhang, T.; Liu, C. Neuroinflammation Mechanisms of Neuromodulation Therapies for Anxiety and Depression. *Transl Psychiatry* **2023**, *13*, 5, doi:10.1038/s41398-022-02297-y.
32. Huang, Y.-Y.; Sharma, S.K.; Carroll, J.; Hamblin, M.R. Biphasic Dose Response in Low Level Light Therapy - an Update. *Dose Response* **2011**, *9*, 602–618, doi:10.2203/dose-response.11-009.Hamblin.
33. Jere, S.W.; Abrahamse, H.; Houreld, N.N. The JAK/STAT Signaling Pathway and Photobiomodulation in Chronic Wound Healing. *Cytokine Growth Factor Rev* **2017**, *38*, 73–79, doi:10.1016/j.cytogfr.2017.10.001.
34. Khan, M.G.M.; Wang, Y. Advances in the Current Understanding of How Low-Dose Radiation Affects the Cell Cycle. *Cells* **2022**, *11*, 356, doi:10.3390/cells11030356.
35. Kitchen, L.C.; Berman, M.; Halper, J.; Chazot, P. Rationale for 1068 Nm Photobiomodulation Therapy (PBMT) as a Novel, Non-Invasive Treatment for COVID-19 and Other Coronaviruses: Roles of NO and Hsp70. *Int J Mol Sci* **2022**, *23*, 5221, doi:10.3390/ijms23095221.

 doi:10.20944/preprints202605.0627.v1

36. Navid, F.; Bruhs, A.; Schuller, W.; Fritsche, E.; Krutmann, J.; Schwarz, T.; Schwarz, A. The Aryl Hydrocarbon Receptor Is Involved in UVR-Induced Immunosuppression. *J Invest Dermatol* **2013**, *133*, 2763–2770, doi:10.1038/jid.2013.221.
37. Ohsugi, Y.; Niimi, H.; Shimohira, T.; Hatasa, M.; Katagiri, S.; Aoki, A.; Iwata, T. In Vitro Cytological Responses against Laser Photobiomodulation for Periodontal Regeneration. *Int J Mol Sci* **2020**, *21*, 9002, doi:10.3390/ijms21239002.
38. Olinski, L.E.; Lin, E.M.; Oancea, E. Illuminating Insights into Opsin 3 Function in the Skin. *Adv Biol Regul* **2020**, *75*, 100668, doi:10.1016/j.jbior.2019.100668.
39. Park, S.; Kim, K.; Bae, I.-H.; Lee, S.H.; Jung, J.; Lee, T.R.; Cho, E.-G. TIMP3 Is a CLOCK-Dependent Diurnal Gene That Inhibits the Expression of UVB-Induced Inflammatory Cytokines in Human Keratinocytes. *FASEB J* **2018**, *32*, 1510–1523, doi:10.1096/fj.201700693R.
40. Rola, P.; Włodarczak, S.; Lesiak, M.; Doroszko, A.; Włodarczak, A. Changes in Cell Biology under the Influence of Low-Level Laser Therapy. *Photonics* **2022**, *9*, 502, doi:10.3390/photonics9070502.
41. Sancar, A. Regulation of the Mammalian Circadian Clock by Cryptochrome. *J Biol Chem* **2004**, *279*, 34079–34082, doi:10.1074/jbc.R400016200.
42. Sklar, L.R.; Almutawa, F.; Lim, H.W.; Hamzavi, I. Effects of Ultraviolet Radiation, Visible Light, and Infrared Radiation on Erythema and Pigmentation: A Review. *Photochem Photobiol Sci* **2013**, *12*, 54–64, doi:10.1039/c2pp25152c.
43. Vieyra-Garcia, P.A.; Wolf, P. From Early Immunomodulatory Triggers to Immunosuppressive Outcome: Therapeutic Implications of the Complex Interplay Between the Wavebands of Sunlight and the Skin. *Front Med (Lausanne)* **2018**, *5*, 232, doi:10.3389/fmed.2018.00232.
44. Wolf, P.; Maier, H.; Müllegger, R.R.; Chadwick, C.A.; Hofmann-Wellenhof, R.; Soyer, H.P.; Hofer, A.; Smolle, J.; Horn, M.; Cerroni, L.; et al. Topical Treatment with Liposomes Containing T4 Endonuclease V Protects Human Skin in Vivo from Ultraviolet-Induced Upregulation of Interleukin-10 and Tumor Necrosis Factor-Alpha. *J Invest Dermatol* **2000**, *114*, 149–156, doi:10.1046/j.1523-1747.2000.00839.x.
45. Wu, S.; Xing, D.; Gao, X.; Chen, W.R. High Fluence Low-Power Laser Irradiation Induces Mitochondrial Permeability Transition Mediated by Reactive Oxygen Species. *J Cell Physiol* **2009**, *218*, 603–611, doi:10.1002/jcp.21636.
46. Yadav, A.; Gupta, A. Noninvasive Red and Near-Infrared Wavelength-Induced Photobiomodulation: Promoting Impaired Cutaneous Wound Healing. *Photodermatol Photoimmunol Photomed* **2017**, *33*, 4–13, doi:10.1111/phpp.12282.
47. Zecha, J.A.E.M.; Raber-Durlacher, J.E.; Nair, R.G.; Epstein, J.B.; Sonis, S.T.; Elad, S.; Hamblin, M.R.; Barasch, A.; Migliorati, C.A.; Milstein, D.M.J.; et al. Low Level Laser Therapy/Photobiomodulation in the Management of Side Effects of Chemoradiation Therapy in Head and Neck Cancer: Part 1: Mechanisms of Action, Dosimetric, and Safety Considerations. *Support Care Cancer* **2016**, *24*, 2781–2792, doi:10.1007/s00520-016-3152-z.
48. Le Novère, N.; Finney, A.; Hucka, M.; Bhalla, U.S.; Campagne, F.; Collado-Vides, J.; Crampin, E.J.; Halstead, M.; Klipp, E.; Mendes, P.; et al. Minimum Information Requested in the Annotation of Biochemical Models (MIRIAM). *Nat Biotechnol* **2005**, *23*, 1509–1515, doi:10.1038/nbt1156.
49. UniProt Consortium UniProt: The Universal Protein Knowledgebase in 2023. *Nucleic Acids Res* **2023**, *51*, D523–D531, doi:10.1093/nar/gkac1052.
50. Schoch, C.L.; Ciufo, S.; Domrachev, M.; Hotton, C.L.; Kannan, S.; Khovanskaya, R.; Leipe, D.; Mcveigh, R.; O'Neill, K.; Robbertse, B.; et al. NCBI Taxonomy: A Comprehensive Update on Curation, Resources and Tools. *Database (Oxford)* **2020**, *2020*, baaa062, doi:10.1093/database/baaa062.
51. Hastings, J.; Owen, G.; Dekker, A.; Ennis, M.; Kale, N.; Muthukrishnan, V.; Turner, S.; Swainston, N.; Mendes, P.; Steinbeck, C. ChEBI in 2016: Improved Services and an Expanding Collection of Metabolites. *Nucleic Acids Res* **2016**, *44*, D1214–D1219, doi:10.1093/nar/gkv1031.
52. Courtot, M.; Juty, N.; Knupfer, C.; Waltemath, D.; Zhukova, A.; Drager, A.; Dumontier, M.; Finney, A.; Golebiewski, M.; Hastings, J.; et al. Controlled Vocabularies and Semantics in Systems Biology. *Molecular systems biology* **2011**, *7*, 543, doi:10.1038/msb.2011.77.

 doi:10.20944/preprints202605.0627.v1

53. Consortium, G.O. Gene Ontology Annotations and Resources. *Nucleic Acids Res* **2013**, *41*, D530-5, doi:10.1093/nar/gks1050.
54. Funahashi, A.; Morohashi, M.; Kitano, H.; Tanimura, N. CellDesigner: A Process Diagram Editor for Gene-Regulatory and Biochemical Networks. *BIOSILICO* **2003**, *1*, 159–162, doi:10.1016/S1478-5382(03)02370-9.
55. Paparozzi, V.; Nardini, C. Tidysbml: R/Bioconductor Package for SBML Extraction into Dataframes. *Bioinformatics Advances* **2024**, *4*, vbae148, doi:10.1093/bioadv/vbae148.
56. Di Lena, P.; Wu, G.; Martelli, P.L.; Casadio, R.; Nardini, C. MIMO: An Efficient Tool for Molecular Interaction Maps Overlap. *BMC bioinformatics* **2013**, *14*, 159, doi:10.1186/1471-2105-14-159.
57. Shannon, P.; Markiel, A.; Ozier, O.; Baliga, N.S.; Wang, J.T.; Ramage, D.; Amin, N.; Schwikowski, B.; Ideker, T. Cytoscape: A Software Environment for Integrated Models of Biomolecular Interaction Networks. *Genome Research* **2003**, *13*, 2498–2504, doi:10.1101/Gr.1239303.
58. Subramanian, A.; Tamayo, P.; Mootha, V.K.; Mukherjee, S.; Ebert, B.L.; Gillette, M.A.; Paulovich, A.; Pomeroy, S.L.; Golub, T.R.; Lander, E.S.; et al. Gene Set Enrichment Analysis: A Knowledge-Based Approach for Interpreting Genome-Wide Expression Profiles. In *Proc Natl Acad Sci U S A*; United States, 2005; Vol. 102, pp. 15545–15550 ISBN 0027-8424 (Print) 0027-8424 (Linking).
59. Fang, Z.; Liu, X.; Peltz, G. GSEApy: A Comprehensive Package for Performing Gene Set Enrichment Analysis in Python. *Bioinformatics* **2023**, *39*, btac757, doi:10.1093/bioinformatics/btac757.
60. Increased Endothelial Mitogen-Activated Protein Kinase Phosphatase-1 Expression Suppresses Proinflammatory Activation at Sites That Are Resistant to Atherosclerosis | Circulation Research Available online: https://www.ahajournals.org/doi/10.1161/CIRCRESAHA.108.183913 (accessed on 6 May 2026).